Hydrogenation-Assisted Graphene Origami and Its Application in Programmable Molecular Mass Uptake, Storage, and Release

Shuze Zhu and Teng Li*

Department of Mechanical Engineering and Maryland NanoCenter, University of Maryland, College Park, Maryland 20742, United States

ABSTRACT The malleable nature of atomically thin graphene makes it a potential candidate material for nanoscale origami, a promising bottom-up nanomanufacturing approach to fabricating nanobuilding blocks of desirable shapes. The success of graphene origami hinges upon precise and facile control of graphene morphology, which still remains as a significant challenge. Inspired by recent progresses on functionalization and patterning of graphene, we demonstrate hydrogenation-assisted graphene origami (HAGO), a feasible and robust approach to enabling the formation of unconventional carbon nanostructures, through systematic molecular dynamics simulations. A unique and desirable feature of HAGO-enabled nanostructures is the programmable tunability of their morphology *via* an external electric field. In particular, we demonstrate reversible opening and closing of a HAGO-enabled graphene nanocage, a mechanism that is crucial to achieve molecular mass uptake, storage, and release. HAGO holds promise to enable an array of carbon nanostructures of desirable functionalities by design. As an example, we demonstrate HAGO-enabled high-density hydrogen storage with a weighted percentage exceeding the ultimate goal of US Department of Energy.

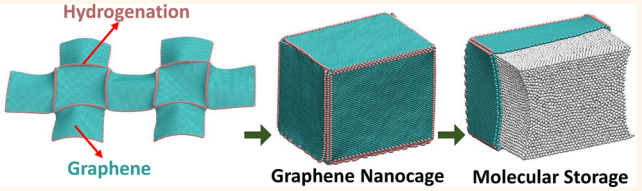

KEYWORDS: graphene · origami · hydrogenation · self-assembly · nanomanufacture

Graphene has emerged as an extraordinary material with its capability to accommodate an array of remarkable electronic, mechanical, and chemical properties.[1−3] Extra-large surface-to-volume ratio renders graphene a highly flexible morphology, giving rise to intriguing observations such as ripples, wrinkles, and folds[4−8] as well as the potential to transform into other novel carbon nanostructures.[8−16] In particular, self-folding of graphene,[8] or graphene origami,[17−19] has been subjected to intensive study due to the need to fabricate unconventional nanostructures *via* approaches beyond conventional material preparation techniques. Progresses in patterning graphene with atomic-scale precision have further paved the way toward achieving graphene origami in a programmable fashion.[18−23] For example, water nanodroplet can activate the self-folding of graphene flake cut in a particular cross shape.[8] The unique feature of such an unconventional bottom-up nanomanufacture technique is that a material building block can self-assemble into a final folded structure, which is typically energetically more favorable and thus more stable than the original building block.[24] In general, nonbonded adhesion, such as van der Waals (vdW) forces, plays a crucial role in overcoming the energy barrier (*e.g.*, bending energy) in order to fold graphene as well as stabilizing the folded nanostructure against the perturbation from thermal fluctuation. A direct example is that a carbon nanoscroll can hold its spiral morphology rather stably *via* vdW forces distributed among interlayers over a large surface area.[8−16] On the other hand, manipulating or neutralizing the interlayer vdW interaction can significantly affect the morphology of the carbon nanoscroll because of its open and tunable topology.[25] By suitably programming the original graphene building blocks, the resulting folded nanostructures of graphene can be customized to take various unique morphology and topology that are otherwise impossible in conventional carbon nanostructures, such as carbon

* Address correspondence to lit@umd.edu.

Received for review January 2, 2014 and accepted February 24, 2014.

Published online February 24, 2014
10.1021/nn500025t

nanotube and fullerene. Such novel nanostructures can overcome some intrinsic difficulties that the conventional carbon nanostructures would inevitably suffer for certain applications. For example, the hollow nature of carbon nanotube[26] and fullerene[27] has motivated the proposal of using such materials as hydrogen storage medium, yet the fact that large size carbon nanotubes and fullerene become structurally unstable poses a practical limitation on storage capacity. By contrast, suitably folded graphene nanostructures can serve as nanocapsules or nanocontainers to host molecular-scale cargo of desirable quantity,[28,29] which has profound implications in molecular vessel and drug delivery applications.[30] For example, as to be shown in this letter, a graphene nanocage can stably store hydrogen molecules with a weighted percentage of 9.7%, exceeding US Department of Energy (DOE)'s ultimate goal of 7.5%.[31]

The two-dimensional nature of graphene makes the chemical functionalization of graphene a promising approach to modulating the graphene properties.[32−38] For example, hydrogenation of graphene[32,39,40] involves bonding atomic hydrogen to the carbon atoms in graphene. Such a reaction changes the hybridization of graphene from sp^2 into sp^3. As a result, the two-dimensional atomic structure of pristine graphene is distorted.[10,11,41] Significant progresses have been achieved on controllable hydrogenation of graphene. For example, single-sided hydrogenation of pristine graphene has been theoretically and experimentally explored.[10,11,32,41−47] Hybrid superlattices made of patterned hydrogenation can be fabricated in a controlled fashion on both macroscopic and microscopic scales.[40] Recent studies show that hydrogen chemisorption in graphene can be enhanced by local curvature in a graphene sheet.[45,48,49] It has also been shown that a graphene sheet can closely conform to the sharp features on a substrate surface (*e.g.*, extrusions and edges),[50−53] leading to large local curvature in the graphene. These findings suggest the feasibility of precise hydrogenation (*e.g.*, in atomic rows) of graphene in a programmable fashion. These advances on programmable bonding of atomic hydrogen to carbon atoms in pristine graphene open up new avenues for manipulating the morphology of graphene and therefore exploring graphene-based novel nanomaterials. In this letter, we use molecular dynamics (MD) simulations to demonstrate the hydrogenation-assisted graphene origami (HAGO), in which initially planar, suitably patterned graphene can self-assemble into three-dimensional nanoscale objects of desirable geometric shapes. We further demonstrate that the HAGO process can be modulated by an external electric field, enabling programmable opening and closing of the resulting three-dimensional nano-objects, a desirable feature to achieve molecular mass manipulation, storage, and delivery. To benchmark this unique feature, we demonstrate using HAGO-enabled nanocage for controllable uptake and release of fullerenes and nanoparticles as well as ultrahigh density of hydrogen storage.

RESULTS AND DISCUSSION

Hydrogenation of a carbon atom in pristine graphene generates an sp^3 carbon−hydrogen (C−H) bond, which induces a local structural change around that carbon atom. The chemically adsorbed hydrogen atom attracts its bonded carbon atom while it repels other neighboring carbon atoms. Therefore, the three initially planar carbon−carbon (C−C) bonds associated with the hydrogenated carbon atom would locally bend away from the hydrogen atom. If the graphene is hydrogenated on both sides, the resulting hydrogenated graphene (termed as graphane[32,39]) would overall remain a rather planar morphology because the local distortions of the C−C bonds neutralize each other. Nevertheless, if the graphene is single-sided hydrogenated, the local distortion at each hydrogenated carbon atom is accumulated.[54] For example, if hydrogenation lines are introduced in one side of a graphene, the accumulated distortion can effectively fold the graphene along the hydrogenation lines to a certain angle. Figure 1 shows that such a folding angle at equilibrium increases when the number of rows of hydrogenation increases. In particular, it is found that the folding angle can be tailored to be close to 90° (*e.g.*, Figure 1(b,e)), which offers the possibility to potentially form a stable folded substructure that consists of two faces that are folded nearly perpendicularly along the hydrogenation lines. The HAGO process often involves a cascade of or simultaneous events of such folding steps, as to be shown below.

Using MD simulations, we have successfully demonstrated an array of unconventional nanostructures enabled by HAGO, including hexahedral nanocage (Figure 2), octohedral nanocage, and nanobusket (Figures S1, S2, Supporting Information). In the simulations, the C−C and C−H bonds in the graphene as well as the nonbonded C−C and C−H interactions are described by AIREBO potential.[55] The simulations are carried out using Large-Scale Atomic/Molecular Massively Parallel Simulator (LAMMPS).[56] Figure 2(a) depicts our simulation model to achieve HAGO-enabled hexahedral graphene nanocage. The double-cross shaped graphene flake is cut out of a rectangular graphene with a length L = 13.2 nm and a width W = 7.1 nm. Rows of single-sided hydrogenation are introduced along the expected edges, which demarcate the graphene flake into nine regions. Hereinafter, each such region is referred to as a graphene wall. Each of the six outer graphene walls (labeled 1−6) has three free edges, and the center graphene wall (labeled 7) has only two free edges, while the remaining two graphene walls (labeled 8 and 9) have no free edges.

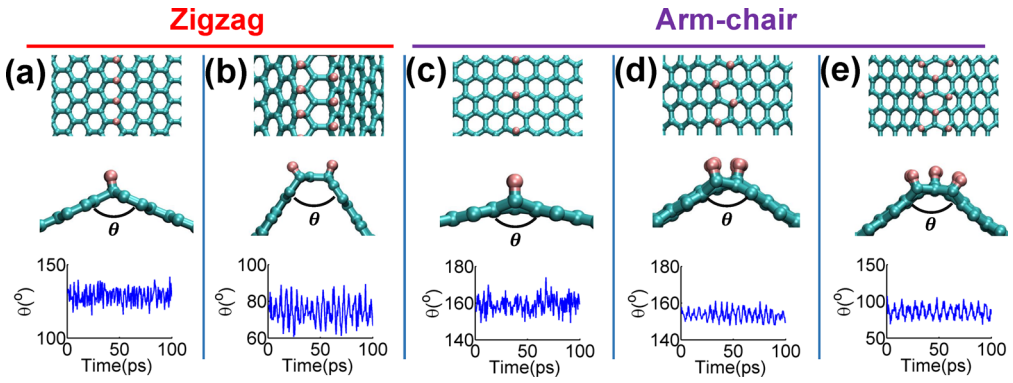

Figure 1. Top view and side view of graphene structures folded to an angle due to single-sided hydrogenation along various lines at equilibrium. (a) One-line and (b) two-line hydrogenation are introduced along zigzag direction of graphene lattice, respectively. (c−e): One-line, two-line, and three-line hydrogenation are introduced along arm-chair direction of graphene lattice, respectively. The bottom row plots the variation of the folding angle at 300 K over time, which is shown to be minimum, indicating robust stability of the folded substructure.

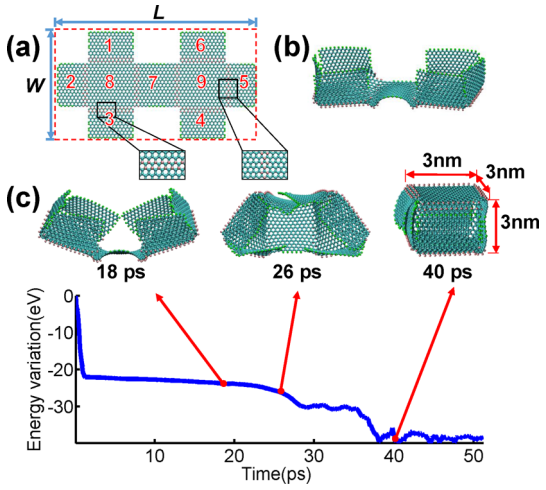

Figure 2. (a) Double-cross shaped graphene flake to achieve HAGO-enabled hexahedral graphene nanocage. Insets show the hydrogenation lines, which demarcate the graphene flake into nine regions (labeled by numbers). (b) Energy-minimized structure by conjugate gradient (CG) and steepest descent algorithm. (c) Further energy minimization toward the formation of a graphene nanocage.

Carbon atoms along the free edges of the graphene flake are saturated by hydrogen atoms to avoid unwanted bond formation during the self-assembling process. Figure 2(b) shows the structural configuration after the initial energy minimization (see Methods and Movie M1 in Supporting Information). Figure 2(c) shows the further structural evolution (see Movie M2 in Supporting Information). At 18 ps, all six outer graphene walls are in the process of bending upward, which later fold along the hydrogenated edges up to about 90°. At 26 ps, the two graphene walls (labeled 8 and 9) are in the process of bending upward, which causes the two sets of folded graphene walls (1−2−3 and 4−5−6) to come close to each other, resembling the closing of a venus flytrap. At 40 ps, the two sets of folded graphene walls overlap with each other. Because of geometrical constraints and interwall vdW interaction, an outer graphene wall on the left slides above or beneath another outer graphene wall on the right. The vdW interaction further drives the tightening of the folded structure and serves as the interwall adhesives to stabilize the final structure. As a result, a quasicubic hexahedral graphene nanocage is formed.

In practice, hydrogenation process of graphene may not be as perfect as the ideal case (*e.g.*, Figure 2(a)). In other words, defective hydrogenation (*e.g.*, missing hydrogen atoms) could occur in a random fashion. To this end, we have carried out further simulations of patterned graphene with random imperfection in hydrogenation. These further studies reveal that HAGO is a rather robust self-assembly process with a strong tolerance to possible imperfect hydrogenation. For example, we show that the graphene nanocage can still be successfully formed even if only less than 70% of single-side hydrogenation from the ideal case is achieved (as detailed in Section IV in Supporting Information).

In the HAGO-enabled graphene nanocage, the interwall vdW interaction energy plays a key role in maintaining the nanocage structural stability. Therefore, manipulation of such an interaction energy potentially offers the morphological tunability of the graphene nanocage (*e.g.*, controllable opening and closing). We next show that an external electric field can effectively reduce the interwall adhesion. Therefore, by tuning the external electric field, facile control of the morphology of graphene nanocage can be achieved. An external electric field can cause the polarization of carbon atoms in graphene. As a result, the intergraphene-layer interaction can be changed. For example, it is shown that an electric field can effectively cause the radial expansion of a carbon nanoscroll due to the polarization-induced decrease of intergraphene-layer adhesion.[25] Recently first-principle calculations have revealed the dependence of the effective dielectric constant in graphene structures on external electric field.[57,58] For a graphene bilayer, both in-plane and out-of-plane

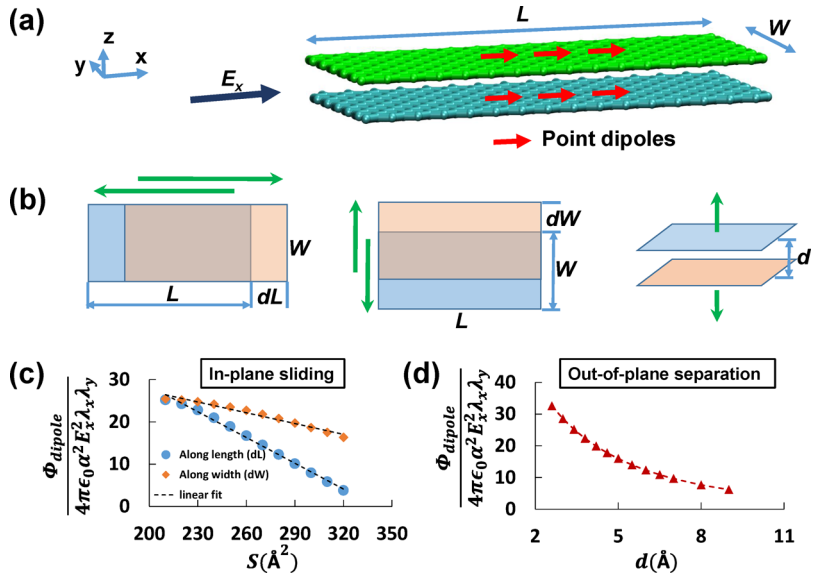

Figure 3. (a) Under an external electric field parallel to the plane of a graphene bilayer, point dipoles of the same direction as the electric field form in the graphene bilayer. (b) Schematics of in-plane sliding (left and middle panels) and out-of-plane separation (right panel) of the graphene bilayer. (c) As the two graphene layers slide off each other in the plane, the normalized dipole−dipole interaction energy decreases as the total surface area of the bilayer (*e.g.*, 2(*L* + d*L*)W or 2*L*(*W* + d*W*)) increases. (d) Similarly, as the two graphene layers separate out-of-plane, such an energy also decreases as the separation distance increases.

polarizations are shown to increase as the electric field increases.[57] When a graphene bilayer is subjected to an out-of-plane electric field, the interlayer adhesion is reported to decrease with increasing electric field intensity, and the two graphene layers can be easily separated when the electric field intensity reaches above 1.8 V/Å.[57] Here we show that the effective interlayer adhesion of a graphene bilayer (*e.g.*, the overlapping walls in the HAGO-enabled graphene nanocage) also decreases when the bilayer is subjected to an electric field parallel to the graphene plane. The effective interlayer adhesion γ_{eff} consists of the contribution of the interlayer vdW interaction and that of the interlayer dipole interaction; *i.e.*, $\gamma_{eff} = \gamma_{vdW} + \gamma_{dipole}$; the dipole-induced surface energy can be deduced as $\gamma_{dipole} = ((d\Phi_{dipole})/dS)$, where Φ_{dipole} is the total dipole−dipole interaction energy and *S* is the total surface area of the graphene (see Section I in Supporting Information). Figure 3(a) shows a schematic of dipole orientations when a graphene bilayer is subjected to an in-plane electric field. Figure 3(c) plots the normalized Φ_{dipole} as a function of *S* as the graphene bilayer slide off each other (*i.e.*, $dS = 2L\,dW$ or $dS = 2W\,dL$, Figure 3(b)). Figure 3(c) shows that Φ_{dipole} monotonically decreases as the interlayer sliding proceeds in two representative directions, indicating that under an in-plane electric field, in-plane sliding of a graphene bilayer is energetically favorable. Figure 3(d) further shows that normalized Φ_{dipole} also decreases as the interlayer separation distance increases, indicating that interlayer out-of-plane separation is also energetically favorable. In addition, the hydrogenation and its induced folding of graphene can also lead to a nonuniform charge distribution (thus global polarization) in the HAGO-enabled graphene nanocage (Figure S6, Supporting Information). We have further shown that such a global polarization can also facilitate the opening of the nanocage when subjected to an external electric field (See Section V in Supporting Information). The above analysis suggests that an external electric field can reduce the effective interwall adhesion in a HAGO-enabled graphene nanocage, a unique feature that can potentially enable facile control of the morphology of graphene nanocage *via* tuning the external electric field.

Inspired by the above feature, we next demonstrate controlled opening and closing of HAGO-enabled graphene nanocage (Figure 4, see Movie M3 in Supporting Information), an otherwise hard to achieve but highly desirable mechanism for molecular mass manipulation. To capture the effect of external electric field on the effective interwall adhesion, the C−C pair potential is represented by a modified Lennard−Jones potential $V_{CC} = 4\lambda_{CC}\varepsilon_{CC}((\sigma_{CC}^{12}/r^{12}) - (\sigma_{CC}^{6}/r^{6}))$, where $\varepsilon_{CC} = 0.00284$ eV, $\sigma_{CC} = 0.34$ nm, and λ_{CC} (≤ 1) is a tuning factor that is to represent the effect of electric field (*e.g.*, $\lambda_{CC} = 1$ when there is no external electric field). As shown in Figure 4, natural vdW interactions facilitate the formation of a closed nanocage, which can be then opened up by applying an external electric field. Upon removing the electric field, the opened graphene nanostructure closes spontaneously, driven by vdW interactions. The controlled opening and closing of the graphene nanocage are reversible and repeatable by turning on and off the external electric field. Such a change of nanocage morphology can be readily understood as

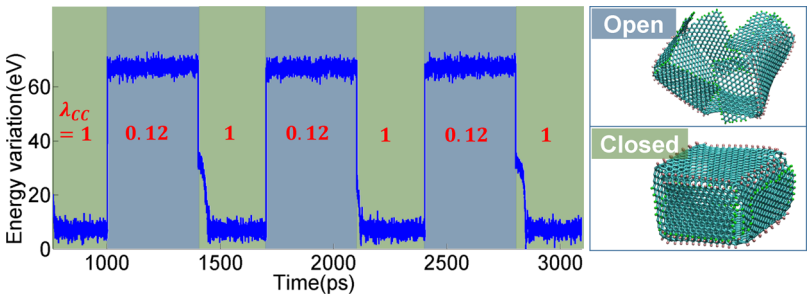

Figure 4. Controlled opening and closing of graphene nanocage *via* tuning effective interwall adhesion. λ_{CC} = 1: without applied electric field, nanocage is closed; λ_{CC} = 0.12: under an applied electric field, interwall adhesion decreases, leading to the opening of the nanocage under thermal fluctuation. The simulation is done in the NVT ensemble at 300 K.

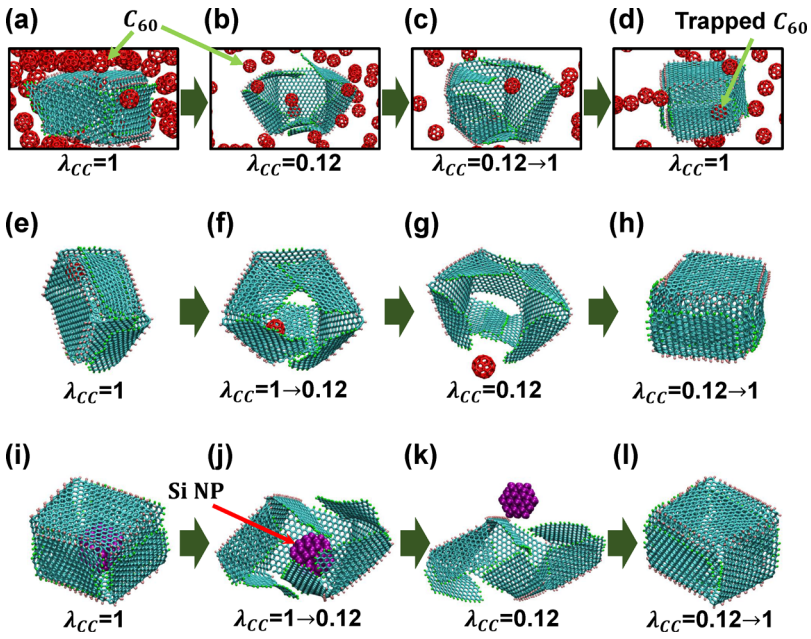

Figure 5. (a–d) Controlled opening and closing of a graphene nanocage immersed in a C_{60} reservoir can enable the uptake of C_{60} molecules by the nanocage. (e–h) After the cargo-loaded nanocage is transported to the destination, the stored C_{60} molecule can be released by the electric field induced opening of the nanocage. (i–l) Release of a silicon nanoparticle from a graphene nanocage under the same mechanism.

follows. In the HAGO-enabled formation of graphene nanocage, the closing of the nanocage leads to the decrease of interwall vdW interaction energy, which counterbalances the increase of folding induced bending energy. On the other hand, subjected to a sufficiently strong electric field, the effective interwall adhesion decreases, to some extent that is not able to hold up the nanocage. As a result, the nanocage opens up to relax the excessive bending energy.

The controlled opening and closing of such graphene nanocages have practical significance, *e.g.*, to be used as a nanovessel or nanocontainer to achieve molecular mass delivery.[28–30] As a demonstration of such a functionality, we study the uptake and release of C_{60} molecules using a HAGO-enabled graphene nanocage. A closed nanocage is first immersed into a reservoir of C_{60} molecules, as shown in Figure 5(a) (see Movie M4 in Supporting Information). The MD simulation using AIREBO potential is carried out with NVT ensemble at a temperature of 300 K.

Reflective wall boundary condition is imposed in all three dimensions of the simulation box to simulate a constant feed of C_{60} molecules. Initially, C_{60} molecules evolve to adhere to the outer surface of the graphene nanocage because of vdW adhesion. When an electric field is applied (*e.g.*, λ_{CC} decreases from 1 to 0.12), the nanocage opens up. Driven by thermal noise, some C_{60} molecules could migrate into the inner space of the nanocage. Upon turning off the electric field, the nanocage closes spontaneously, and these C_{60} molecules are uptaken and stored inside the nanocage (Figure 5(a–d), see Movie M4 in Supporting Information). After the nanocage with the cargo load (*e.g.*, C_{60}) is transported to a designated destination, release of the cargo load can be achieved by applying an electric field to open up the nanocage, followed by the migration of the C_{60} molecules out of the nanocage

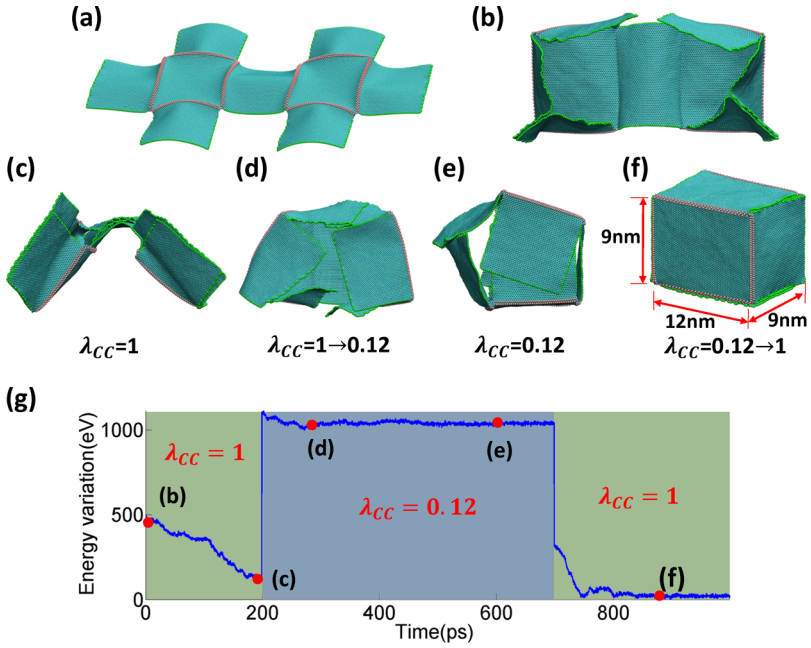

Figure 6. (a) Patterned graphene is suitably hydrogenated to form a graphene nanocage of large size. (b) Morphology after initial energy minimization. (c–f) Electric field assisted formation of large size graphene nanocage. (g) Evolution of potential energy from (b–f), indicating that the electric field can help prevent the graphene nanostructure trapped in unwanted metastable state (c) and facilitate the formation of the final nanocage (f), a thermodynamically stable state.

driven by thermal fluctuation (Figure 5(e–h), see Movie M5 in Supporting Information). We have also demonstrated the uptake and release of other molecular mass (*e.g.*, silicon nanoparticles, Figure 5(i–l)) using the HAGO-enabled graphene nanocage under the same mechanisms. Note that, despite the possible uncertainty of the thermally driven process, programmable uptake, storage, and release of molecular mass could be implemented by controlling a large amount of HAGO-enabled graphene nanocages *via* a global electric field.

An external electric field can also facilitate the formation of graphene nanocages of large sizes that are otherwise challenging to achieve. Figure 6 shows the electric field assisted formation of a graphene nanocage with a size of 9 nm by 9 nm by 12 nm. Figure 6(a,b) shows two snapshots during the energy minimization process. When the graphene flake becomes larger, it becomes easier to fluctuate out-of-plane. As a result, neighboring graphene walls evolve to partially attach to each other driven by vdW adhesion, preventing the desirable formation of a nanocage. Such an unwanted feature can be overcome by the help of external electric field. As shown in Figure 6(d–f), upon applying an electric field followed by turning it off, the initially collapsed graphene structure first partially opens up and finally folds up into a rather regular hexahedron nanocage (see Movie M6 in Supporting Information). The effect of the electric field in such a process can be understood as follows. In the presence of an electric field, the effective interwall adhesion decreases, which cannot balance the excessive bending energy in the initially collapsed and distorted graphene structure. As a result, the entire graphene structure first partially opens up to release excessive bending energy and then gradually evolves toward lower energy configuration (Figure 6(d,e)). After such a priming process and followed by restoring the natural interwall vdW adhesion by turning off the electric field, the graphene structure finally evolves into a regular nanocage as desired, which corresponds to the lowest energy level as shown in Figure 6(g). In other words, the electric field can help prevent the graphene structure getting stuck in unwanted metastable states and thus facilitate the formation of the thermodynamically stable graphene nanostructure. Results in Figure 6 further demonstrate the feasibility and robustness of the programmable HAGO process.

The tunable and robust morphology HAGO-enabled graphene nanocage as well as its hollow nature with a volumetric capacity of nearly 1000 nm^3 (*e.g.*, Figure 6(f)) render attractive attributes for potential applications such as nanoscale pressure tank.[26,27] To benchmark such potentials, here we demonstrate high density hydrogen storage enabled by graphene. Giant fullerenes have been proposed to serve as a medium of high density hydrogen storage,[27] but their closed nature poses an intrinsic challenge to uptake and release hydrogen, as such a processes involve breaking covalent C–C bonds and thus are irreversible. By contrast, a HAGO-enabled graphene nanocage can be repeatedly opened and closed *via* facile control of an external electric field, making reversible uptake and release of hydrogen feasible. Although the graphene nanocage is not fully sealed by covalent bonds as in a giant

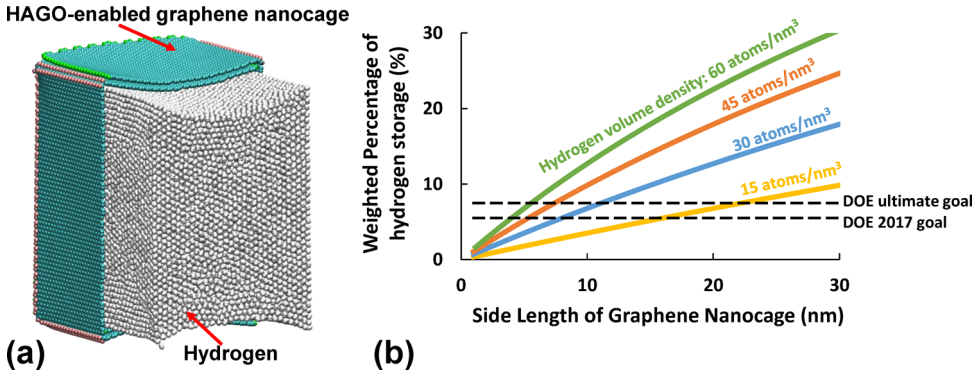

Figure 7. (a) High density hydrogen storage in HAGO-enabled graphene nanocage, with a weighted percentage of 9.7%, beyond the US DOE ultimate goal of 7.5% for hydrogen storage. For visual clarity, only half of the nanocage is shown. See Movie M7 in Supporting Information. (b) Weighted percentage of hydrogen storage in HAGO-enabled graphene nanocage as a function of the side length of a cubic graphene nanocage, for four different hydrogen volume densities inside the nanocage. Dashed lines denote US DOE ultimate goal and year 2017 goal on hydrogen storage density.

fullerene, the interwall adhesion over large areas indeed allows it to sustain sufficiently high pressure (thus store a large amount of hydrogen molecules inside). In addition, when an empty nanocage is immersed in a hydrogen reservoir, a slight opening of the nanocage effectively gives rise to the formation of gaps or pores along the edge and corner of the nanocage, a feature that allows the adsorption of hydrogen atoms into the inner volume of the nanocage (See Section VI in Supporting Information).[59,60]

As shown in Figure 7(a) (see Movie M7 in Supporting Information), the graphene nanocage in Figure 6 can host 47 880 hydrogen atoms in its inner volume at a temperature of 70 K. During the MD simulation, no escaping of the hydrogen is observed at such a temperature. The graphene nanocage contains 37 130 carbon atoms and 1468 initially chemically adsorbed hydrogen atoms. Therefore, the weighted percentage of the hydrogen storage is about 9.7%, which exceeds the US DOE target of 5.5% for the year 2017 and the ultimate goal of 7.5%,[31] indicating the promising potential of HAGO-enabled graphene nanocage as a high density hydrogen storage medium. The hydrogen storage density using graphene nanocage depends on the nanocage size, which can be estimated by a simple model. Consider a cubic graphene nanocage formed *via* HAGO process with side length of L, let ρ_c be the *area* density of graphene, ρ_h be the volume density of the stored hydrogen, m_h and m_c be the atomic mass of hydrogen and carbon atoms, respectively. The weighted percentage of hydrogen storage in such a graphene nanocage can be estimated by $((m_h\rho_h L^3)/(m_h\rho_h L^3 + 9m_c\rho_c L^2))$. Figure 7(b) plots the weighted percentage of hydrogen storage as a function of graphene nanocage size L, for four different hydrogen volume density. As shown in Figure 7(b), the hydrogen storage capacity increases as the graphene nanocage size increases, in an approximately linear fashion. For example, to reach the DOE's ultimate goal for hydrogen storage density, graphene nanocages of size greater than 12 and 6 nm are needed, for the hydrogen volume density of 30 and 60 atom/nm^3, respectively. We have also shown that such hydrogen volume density levels can be feasibly achieved by tuning the ambient hydrogen reservoir pressure (see Section VI in Supporting Information). In this sense, the above estimation offers a rule-of-thumb guideline for the design of graphene nanocage to achieve certain hydrogen storage density. The hydrogen atoms stored inside the graphene nanocage can also be effectively released by elevating the temperature (details available in Section VII in Supporting Information).

CONCLUSIONS

In summary, through systematic MD simulations, we demonstrate a feasible and robust hydrogenation-assisted graphene origami (HAGO) process. We further reveal that a HAGO-enabled graphene nanocage can be reversibly opened and closed in a programmable fashion *via* the facile control of an external electric field, a desirable feature that can enable controllable molecular mass uptake, storage, and release, as well as high density hydrogen storage. These promising applications of HAGO process and HAGO-enabled novel nanostructures call for further experimental investigations to explore their full potential.

METHODS

C−C and C−H bonds in the graphene as well as the nonbonded C−C and C−H interactions are described by AIREBO potential.[55] The simulations are carried out using Large-Scale Atomic/Molecular Massively Parallel Simulator (LAMMPS).[56] The time step for all simulations is set to be 0.5 femtoseconds (fs). Molecular dynamics simulations in Figure 1, Figure 4, Figure 5, and Figure 6(c−f) are done in NVT ensemble at 300 K and by Nose−Hoover thermostat. Molecular dynamics simulations in

Figure 7(a) are done in NVT ensemble at 70 K and by Nose–Hoover thermostat. Figure 2 is to demonstrate that HAGO is intrinsically energetically favorable; therefore, energy minimization simulations are done in NVE ensemble (not NVT) in Figure 2. Energy minimization simulations in Figure 2 (also in Figure 6(a,b)) are first done by conjugate gradient (CG) algorithm followed by steepest descent algorithm until either the total energy change between successive iterations divided by the energy magnitude is less than or equal to 10^{-10} or the total force is less than 10^{-5} eV Å^{-1}. However, both conjugate gradient and steepest descent algorithm are highly possible to find a local energy minimum point. To gain further approach to global energy minimum configuration, we adopted an alternate way of relaxing a system by running dynamics with a small or limited time step.[56] The simulation is then running in NVE ensemble with the restriction that the maximum distance an atom can move in one time step is 0.1 Å. The time step is set to be 0.5 fs.

Conflict of Interest: The authors declare no competing financial interest.

Acknowledgment. This research is supported by the National Science Foundation (Grant Numbers: 1069076 and 1129826). Z.S. is thankful for the support of the Clark School Future Faculty Program at the University of Maryland.

Supporting Information Available: Details of theoretical method, other forms of HAGO-enabled nanostructures, effect of imperfection in hydrogenation pattern, effect of global polarization, hydrogen adsorption into graphene nanocage, and temperature-modulated hydrogen release. Supporting figures and videos. This material is available free of charge *via* the Internet at http://pubs.acs.org.

REFERENCES AND NOTES

1. Geim, A.; Novoselov, K. The Rise of Graphene. *Nat. Mater.* **2007**, *6*, 183–191.
2. Klimov, N. N.; Jung, S.; Zhu, S.; Li, T.; Wright, C. A.; Solares, S. D.; Newell, D. B.; Zhitenev, N. B.; Stroscio, J. A. Electromechanical Properties of Graphene Drumheads. *Science* **2012**, *336*, 1557–1561.
3. Lee, C.; Wei, X.; Kysar, J.; Hone, J. Measurement of the Elastic Properties and Intrinsic Strength of Monolayer Graphene. *Science* **2008**, *321*, 385–388.
4. Fasolino, A.; Los, J.; Katsnelson, M. Intrinsic Ripples in Graphene. *Nat. Mater.* **2007**, *6*, 858–861.
5. Zhu, S.; Galginaitis, J.; Li, T. Critical Dispersion Distance of Silicon Nanoparticles Intercalated Between Graphene Layers. *J. Nanomater.* **2012**, 375289(1)–375289(4), DOI: 10.1155/2012/375289.
6. Li, T. Extrinsic Morphology of Graphene. *Modell. Simul. Mater. Sci. Eng.* **2011**, *19*, 054005(1)–054005(15).
7. Kim, K.; Lee, Z.; Malone, B.; Chan, K.; Aleman, B.; Regan, W.; Gannett, W.; Crommie, M.; Cohen, M.; Zettl, A. Multiply Folded Graphene. *Phys. Rev. B: Condens. Matter Mater. Phys.* **2011**, *83*, 245433(1)–245433(8).
8. Patra, N.; Wang, B.; Kral, P. Nanodroplet Activated and Guided Folding of Graphene Nanostructures. *Nano Lett.* **2009**, *9*, 3766–3771.
9. Zhang, Z.; Li, T. Carbon Nanotube Initiated Formation of Carbon Nanoscrolls. *Appl. Phys. Lett.* **2010**, *97*, 081909(1)–081909(3).
10. Zhu, S.; Li, T. Hydrogenation Enabled Scrolling of Graphene. *J. Phys. D: Appl. Phys.* **2013**, *46*, 075301(1)–075301(8).
11. Yu, D.; Liu, F. Synthesis of Carbon Nanotubes by Rolling up Patterned Graphene Nanoribbons Using Selective Atomic Adsorption. *Nano Lett.* **2007**, *7*, 3046–3050.
12. Zhang, Z.; Li, T. Ultrafast Nano-Oscillators Based on Interlayer-Bridged Carbon Nanoscrolls. *Nanoscale Res. Lett.* **2011**, *6*, 470(1)–470(11).
13. Shi, X.; Pugno, N.; Gao, H. Tunable Core Size of Carbon Nanoscrolls. *J. Comput. Theor. Nanosci.* **2010**, *7*, 517–521.
14. Xie, X.; Ju, L.; Feng, X.; Sun, Y.; Zhou, R.; Liu, K.; Fan, S.; Li, Q.; Jiang, K. Controlled Fabrication of High-Quality Carbon Nanoscrolls from Monolayer Graphene. *Nano Lett.* **2009**, *9*, 2565–2570.
15. Braga, S.; Coluci, V.; Legoas, S.; Giro, R.; Galvao, D.; Baughman, R. Structure and Dynamics of Carbon Nanoscrolls. *Nano Lett.* **2004**, *4*, 881–884.
16. Martins, B.; Galvao, D. Curved Graphene Nanoribbons: Structure and Dynamics of Carbon Nanobelts. *Nanotechnology* **2010**, *21*, 075710(1)–075710(6).
17. Siegel, J. Materials Chemistry: Carbon Origami. *Nature* **2012**, *486*, 327–328.
18. Feng, J.; Li, W.; Qian, X.; Qi, J.; Qi, L.; Li, J. Patterning of Graphene. *Nanoscale* **2012**, *4*, 4883–4899.
19. Qi, J.; Huang, J.; Feng, J.; Shi, D.; Li, J. The Possibility of Chemically Inert, Graphene-Based All-Carbon Electronic Devices with 0.8 eV Gap. *ACS Nano* **2011**, *5*, 3475–3482.
20. Bell, D.; Lemme, M.; Stern, L.; Williams, J. R.; Marcus, C. Precision Cutting and Patterning of Graphene with Helium Ions. *Nanotechnology* **2009**, *20*, 455301(1)–455301(5).
21. Ci, L.; Xu, Z.; Wang, L.; Gao, W.; Ding, F.; Kelly, K.; Yakobson, B.; Ajayan, P. Controlled Nanocutting of Graphene. *Nano Res.* **2008**, *1*, 116–122.
22. Ci, L.; Song, L.; Jariwala, D.; Elias, A.; Gao, W.; Terrones, M.; Ajayan, P. Graphene Shape Control by Multistage Cutting and Transfer. *Adv. Mater.* **2009**, *21*, 4487–4491.
23. Fischbein, M.; Drndic, M. Electron Beam Nanosculpting of Suspended Graphene Sheets. *Appl. Phys. Lett.* **2008**, *93*, 113107(1)–113107(3).
24. Whitesides, G. Nanoscience, Nanotechnology, and Chemistry. *Small* **2005**, *1*, 172–179.
25. Shi, X.; Cheng, Y.; Pugno, N.; Gao, H. Tunable Water Channels with Carbon Nanoscrolls. *Small* **2010**, *6*, 739–744.
26. Chen, H.; Sun, D.; Gong, X.; Liu, Z. Self-Assembled Water Molecules as a Functional Valve for a High-Pressure Nanocontainer. *Angew. Chem., Int. Ed.* **2013**, *52*, 1973–1976.
27. Pupysheva, O.; Farajian, A.; Yakobson, B. Fullerene Nanocage Capacity for Hydrogen Storage. *Nano Lett.* **2008**, *8*, 767–774.
28. Chen, Y.; Guo, F.; Jachak, A.; Kim, S.; Datta, D.; Liu, J.; Kulaots, I.; Vaslet, C.; Jang, H.; Huang, J.; Kane, A.; Shenoy, V.; Hurt, R. Aerosol Synthesis of Cargo-Filled Graphene Nanosacks. *Nano Lett.* **2012**, *12*, 1996–2002.
29. Chen, Y.; Guo, F.; Qiu, Y.; Hu, H.; Kulaots, I.; Walsh, E.; Hurt, R. Encapsulation of Particle Ensembles in Graphene Nanosacks as a New Route to Multifunctional Materials. *ACS Nano* **2013**, *7*, 3744–3753.
30. Fernandes, R.; Gracias, D. Self-Folding Polymeric Containers for Encapsulation and Delivery of Drugs. *Adv. Drug Delivery Rev.* **2012**, *64*, 1579–1589.
31. DOE, Office of Energy Efficiency and Renewable Energy (EERE). http://www1.eere.energy.gov/hydrogenandfuelcells/storage/pdfs/targets_onboard_hydro_storage.pdf, 2009.
32. Elias, D.; Nair, R.; Mohiuddin, T.; Morozov, S.; Blake, P.; Halsall, M.; Ferrari, A.; Boukhvalov, D.; Katsnelson, M.; Geim, A.; Novoselov, K. Control of Graphene's Properties by Reversible Hydrogenation: Evidence for Graphane. *Science* **2009**, *323*, 610–613.
33. Xu, Y.; Bai, H.; Lu, G.; Li, C.; Shi, G. Flexible Graphene Films *via* the Filtration of Water-Soluble Noncovalent Functionalized Graphene Sheets. *J. Am. Chem. Soc.* **2008**, *130*, 5856–5857.
34. Ryu, S.; Han, M.; Maultzsch, J.; Heinz, T.; Kim, P.; Steigerwald, M.; Brus, L. Reversible Basal Plane Hydrogenation of Graphene. *Nano Lett.* **2008**, *8*, 4597–4602.
35. Wang, X.; Tabakman, S.; Dai, H. Atomic Layer Deposition of Metal Oxides on Pristine and Functionalized Graphene. *J. Am. Chem. Soc.* **2008**, *130*, 8152–8153.
36. Boukhvalov, D.; Katsnelson, M. Chemical Functionalization of Graphene with Defects. *Nano Lett.* **2008**, *8*, 4373–4379.
37. Boukhvalov, D.; Katsnelson, M.; Lichtenstein, A. Hydrogen on Graphene: Electronic Structure, Total energy, Structural Distortions and Magnetism from First-Principles Calculations. *Phys. Rev. B: Condens. Matter Mater. Phys.* **2008**, *77*, 035427(1)–035427(7).
38. Balog, R.; Jorgensen, B.; Nilsson, L.; Andersen, M.; Rienks, E.; Bianchi, M.; Fanetti, M.; Laegsgaard, E.; Baraldi, A.; Lizzit, S.;

Sljivancanin, Z.; Besenbacher, F.; Hammer, B.; Pedersen, T.; Hofmann, P.; Hornekaer, L. Bandgap Opening in Graphene Induced by Patterned Hydrogen Adsorption. *Nat. Mater.* **2010**, *9*, 315–319.
39. Sofo, J.; Chaudhari, A.; Barber, G. Graphane: A Two-Dimensional Hydrocarbon. *Phys. Rev. B: Condens. Matter Mater. Phys.* **2007**, *75*, 153401(1)–153401(4).
40. Sun, Z.; Pint, C.; Marcano, D.; Zhang, C.; Yao, J.; Ruan, G.; Yan, Z.; Zhu, Y.; Hauge, R.; Tour, J. Towards Hybrid Superlattices in Graphene. *Nat. Commun.* **2011**, *2*, 559(1)–559(5).
41. Reddy, C.; Zhang, Y.; Shenoy, V. Patterned Graphone—A Novel Template for Molecular Packing. *Nanotechnology* **2012**, *23*, 165303(1)–165303(5).
42. Pujari, B.; Gusarov, S.; Brett, M.; Kovalenko, A. Single-Side-Hydrogenated Graphene: Density Functional Theory Predictions. *Phys. Rev. B: Condens. Matter Mater. Phys.* **2011**, *84*, 041402(R)(1)–041402(R)(4).
43. Zhou, J.; Wang, Q.; Sun, Q.; Chen, X.; Kawazoe, Y.; Jena, P. Ferromagnetism in Semihydrogenated Graphene Sheet. *Nano Lett.* **2009**, *9*, 3867–3870.
44. Sessi, P.; Guest, J.; Bode, M.; Guisinger, N. Patterning Graphene at the Nanometer Scale *via* Hydrogen Desorption. *Nano Lett.* **2009**, *9*, 4343–4347.
45. Chernozatonskii, L.; Sorokin, P. Nanoengineering Structures on Graphene with Adsorbed Hydrogen "Lines". *J. Phys. Chem. C* **2010**, *114*, 3225–3229.
46. Zhang, H.; Miyamoto, Y.; Rubio, A. Laser-Induced Preferential Dehydrogenation of Graphane. *Phys. Rev. B: Condens. Matter Mater. Phys.* **2012**, *85*, 201409(R)(1)–201409(R)(4).
47. Zhou, J.; Sun, Q. How to Fabricate a Semihydrogenated Graphene Sheet? A Promising Strategy Explored. *Appl. Phys. Lett.* **2012**, *101*, 073114(1)–073114(4).
48. Tada, K.; Furuya, S.; Watanabe, K. *Ab Initio* Study of Hydrogen Adsorption to Single-Walled Carbon Nanotubes. *Phys. Rev. B: Condens. Matter Mater. Phys.* **2001**, *63*, 155405(1)–155405(4).
49. Ruffieux, P.; Groning, O.; Bielmann, M.; Mauron, P.; Schlapbach, L.; Groning, P. Hydrogen Adsorption on Sp^2-Bonded Carbon: Influence of the Local Curvature. *Phys. Rev. B: Condens. Matter Mater. Phys.* **2002**, *66*, 245416(1)–245416(8).
50. Lui, C.; Liu, L.; Mak, K.; Flynn, G.; Heinz, T. Ultraflat Graphene. *Nature* **2009**, *462*, 339–341.
51. Ishigami, M.; Chen, J.; Cullen, W.; Fuhrer, M.; Williams, E. Atomic Structure of Graphene on SiO_2. *Nano Lett.* **2007**, *7*, 1643–1648.
52. Zhu, S.; Li, T. Wrinkling Instability of Graphene on Substrate-Supported Nanoparticles. *J. Appl. Mech.* **2014**, *81*, 061008(1)–061008(5).
53. Yamamoto, M.; Pierre-Louis, O.; Huang, J.; Fuhrer, M.; Einstein, T.; Cullen, W. "The Princess and the Pea" at the Nanoscale: Wrinkling and Delamination of Graphene on Nanoparticles. *Phys. Rev. X* **2012**, *2*, 041018(1)–041018(11).
54. Zhang, Z.; Liu, B.; Hwang, K.; Gao, H. Surface-Adsorption-Induced Bending Behaviors of Graphene Nanoribbons. *Appl. Phys. Lett.* **2011**, *98*, 121909(1)–121909(3).
55. Stuart, S.; Tutein, A.; Harrison, J. A Reactive Potential for Hydrocarbons with Intermolecular Interactions. *J. Chem. Phys.* **2000**, *112*, 6472–6486.
56. Plimpton, S. Fast Parallel Algorithms for Short-Range Molecular-Dynamics. *J. Comput. Phys.* **1995**, *117*, 1–19.
57. Santos, E.; Kaxiras, E. Electric-Field Dependence of the Effective Dielectric Constant in Graphene. *Nano Lett.* **2013**, *13*, 898–902.
58. Santos, E. Magnetoelectric Effect in Functionalized Few-Layer Graphene. *Phys. Rev. B: Condens. Matter Mater. Phys.* **2013**, *87*, 155440(1)–155440(7).
59. Gogotsi, Y.; Dash, R.; Yushin, G.; Yildirim, T.; Laudisio, G.; Fischer, J. Tailoring of Nanoscale Porosity in Carbide-Derived Carbons for Hydrogen Storage. *J. Am. Chem. Soc.* **2005**, *127*, 16006–16007.
60. Yushin, G.; Dash, R.; Jagiello, J.; Fischer, J.; Gogotsi, Y. Carbide-Derived Carbons: Effect of Pore Size on Hydrogen Uptake and Heat of Adsorption. *Adv. Funct. Mater.* **2006**, *16*, 2288–2293.

Supporting Information

Hydrogenation Assisted Graphene Origami and Its Application in Programmable Molecular Mass Uptake, Storage, and Release

Shuze Zhu, Teng Li*

Department of Mechanical Engineering and Maryland NanoCenter, University of Maryland, College Park, MD 20742

*Corresponding author: LiT@umd.edu

I. Dipole-dipole interaction

The dipole-dipole interactions[S1] can be described as $V(\vec{r}_{ij}) = \frac{1}{4\pi\epsilon_0|\vec{r}_{ij}|^3}\left[|\vec{p}_i||\vec{p}_j| - \frac{3(\vec{r}_{ij}\cdot\vec{p}_i)(\vec{r}_{ij}\cdot\vec{p}_j)}{|\vec{r}_{ij}|^2}\right]$, where $\vec{r}_{ij}$ is the distance between dipole i and dipole j, $\vec{p}_i = 4\pi\epsilon_0\alpha_i\vec{E}$ the induced dipole mement, $\vec{E}$ the applied electric field, ϵ_0 the vacuum permittivity, and α_i the polarizability of atom i. Assume $\vec{E} = (E_x, 0, 0)$ and the carbon planes are in parallel with the electric field. Only the dipole-dipole interaction between two layers is considered because they are expected to act against the vdW adhesion the most. Let $\vec{r}_{ij} = (x_j - x_i, y_j - y_i, z_j - z_i)$ and assuming constant polarizability for each carbon atom $\alpha_i = \alpha_j = \alpha$, we have

$V(\vec{r}_{ij}) = \frac{4\pi\epsilon_0\alpha^2E_x^2}{\left((x_i-x_j)^2+(y_i-y_j)^2+d^2\right)^{\frac{3}{2}}} - \frac{12\pi\epsilon_0\alpha^2E_x^2(x_j-x_i)^2}{\left((x_i-x_j)^2+(y_i-y_j)^2+d^2\right)^{\frac{5}{2}}}$, where d denotes the interlayer spacing.

The total dipole-dipole interaction energy is $\Phi_{dipole} = \sum_{i\neq j} V(\vec{r}_{ij})$, from which the dipole-induced surface energy can be deduced as $\gamma_{dipole} = \frac{d\Phi_{dipole}}{dS} = \frac{d\Phi_{dipole}}{2(WdL+LdW)}$. The total dipole-dipole interaction energy can be calculated as

$$\Phi_{\text{dipole}} = \lambda_x \lambda_y \int_{x_1 min}^{x_1 max} \int_{x_2 min}^{x_2 max} \int_{y_1 min}^{y_1 max} \int_{y_2 min}^{y_2 max} \frac{4\pi\epsilon_0 \alpha^2 E_x^2}{((x_1 - x_2)^2 + (y_1 - y_2)^2 + d^2)^{\frac{3}{2}}}$$

$$- \frac{12\pi\epsilon_0 \alpha^2 E_x^2 (x_2 - x_1)^2}{((x_1 - x_2)^2 + (y_1 - y_2)^2 + d^2)^{\frac{5}{2}}} dx_1 dx_2 \, dy_1 dy_2$$

where $\lambda_x$and λ_y are the dipole density along x and y direction.

II. Formation of octohedral nanocage

We demonstrate the HAGO-enabled formation of octahedral graphene nanocage. A graphene bilayer is patterned into a shape with four triangular flaps and its outer surface is suitably hydrogenated, as shown in Figure S1 (a). Different from those in the case of forming hexahedron graphene nanocage, all free edges in the graphene bilayer are not saturated by hydrogen atoms to allow the desirable bonding formation to seal the edges. The initial separation distance between the two graphene layers is 0.34 nm and the simulation is carried out with Canonical Ensemble at a temperature of 900K to facilitate the covalent bonding formation between neighboring free edges. Single-sided hydrogenation in the center region leads to accumulated distortion of each graphene layer (Figure S1 (b)). As a result, the center region of each graphene layer bulges out and separate, causing the four triangle flaps in the top graphene layer curve down and those in the bottom layer curve up. When the free side edges of neighboring triangle flaps come close to each other, covalent bonds form between the unsaturated carbon atoms along the free edges (Figure S1 (c)). Meanwhile, the four basal edges in the top graphene layer also bond with the corresponding four basal edges in the bottom graphene layer, as the curving of both layers occurs. Finally, an octahedron graphene nanocage with closed topology is formed. (Figure S1 (d)). If needed, the resulting nanocage can undergo a thermal dehydrogenation process. The temperature

is first gradually increased to 1400K in 100 picoseconds and maintained at 1400K for another 100 picosecond to allow the hydrogen atoms to desorb from the graphene completely. Then the temperature is cooling down to 300K gradually in 100 picoseconds. The temperature is

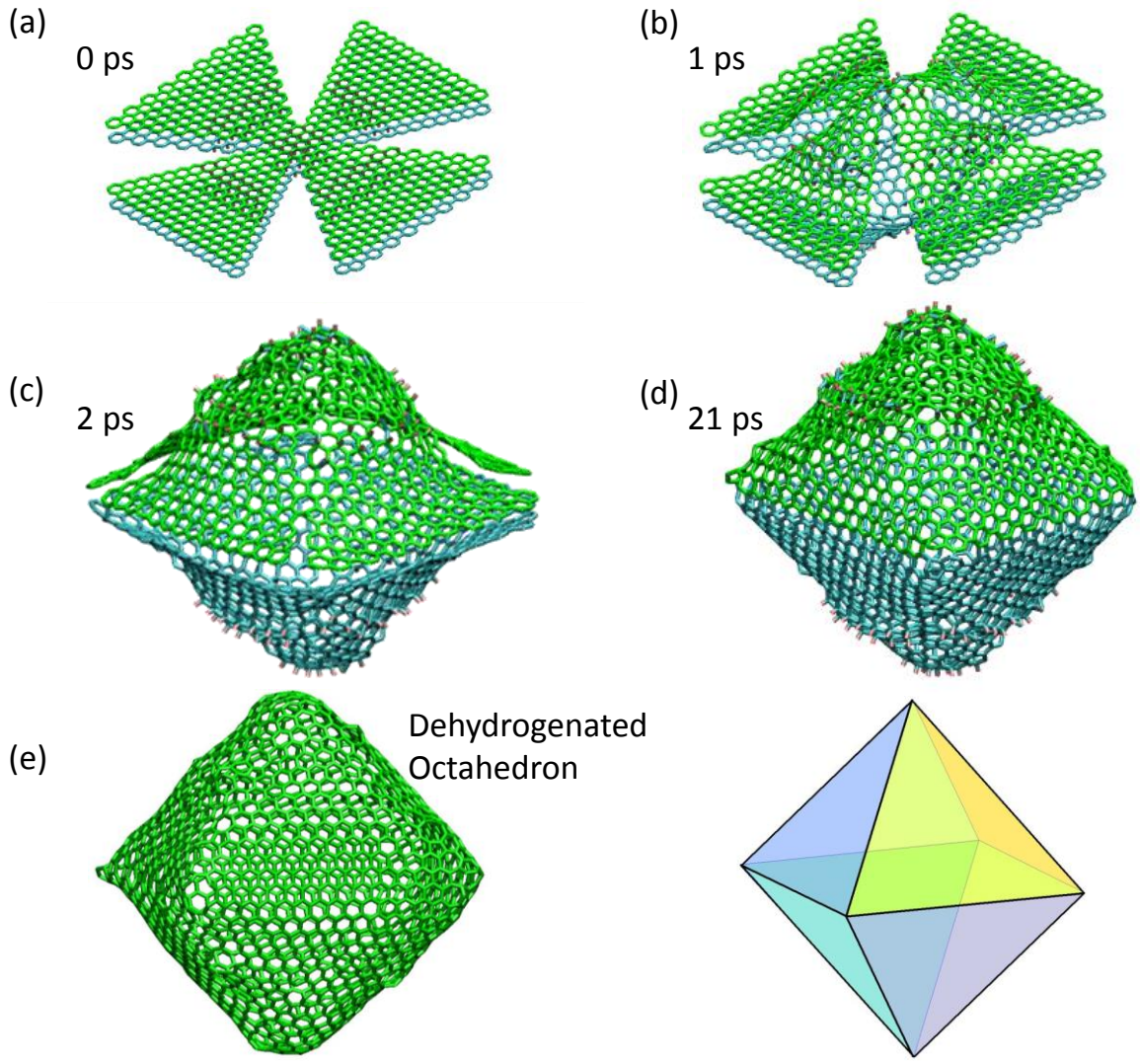

Figure S1. *Snapshots of the formation of octahedron graphene nanocage and resultant hydrogen-free nanostructure after dehydrogenation. (a) Initial configuration. (b) Single-sided hydrogenation causes the central parts to bulge out and separate. (c) As neighboring free edges come close to each other, covalent bonds form to seal the edges, leading to an octahedron graphene nanocage (d). Further dehydrogenation can result in a hydrogen-free octahedron graphene nanocage (e).*

controlled by a Nose-Hoover thermostat and is relaxed every 0.1 picosecond. The resulting hydrogen-free octahedron graphene nanocage is shown in Figure S1 (e).

III. Formation of a graphene nanobusket

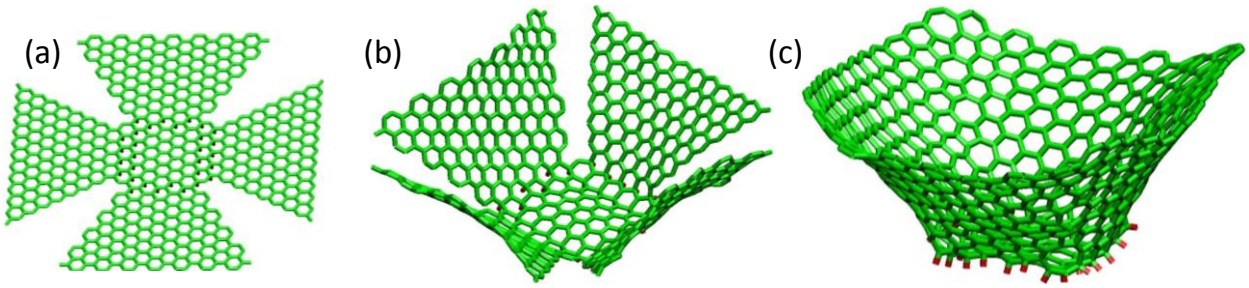

Figure S2. *Snapshots of the formation of a graphene nanobasket.*

We further show the formation of a graphene nanobasket, as shown in Figure S2. The molecular dynamics simulation is carried out with Canonical Ensemble at a temperature of 900K. A monolayer graphene is first patterned into a shape of four trapezoidal flaps connecting to a square base (Figure S2 (a)). Two rows of hydrogenation are introduced along the four sides of the central square base. The hydrogenation induced bending causes the four flaps to curve up and come close to each other, so that covalent bonds form between neighboring free edges, leading to the formation of a stable graphene nanobasket (Figure S2 (c)).

IV. Effect of imperfection in hydrogenation pattern on HAGO

We further investigate the formation of graphene nanocage with the influence of the defective hydrogenation. To this end, we employ the same simulation methodology as in Figure 2 in order to make direct comparison. As a reference, Figure S3 (a) shows the complete hydrogenation pattern as in Figure 2 with 184 hydrogen atoms (the carbon atoms are not shown for visual

clarity). Defective hydrogenation patterns are generated by randomly removing hydrogen atoms from the complete hydrogenation pattern. Three defective levels are considered, with 20, 40 and 56 hydrogen atoms removed from the complete hydrogenation pattern, corresponding to the perfection rate of 89.2% (Figure S4 (a)), 78.3% (Figure S4 (b)) and 69.6% (Figure S3 (b)), respectively. It turns out that in all three cases of defective hydrogenation, the HAGO-driven formation of graphene nanocage can still be achieved. Figure S3 (e) plots the sequential snapshots of the nanocage formation and the corresponding energy evolution for the case of perfection rate of 69.6%, which reveal a process quite similar with the case of complete hydrogenation as shown in Figure 2. Figure S4 (a) and (b) further show the final shape of the nanocages formed under the hydrogenation perfection rate of 89.2% and 78.3%, respectively. No appreciable difference in the final shapes is found in all simulation cases once the graphene nanocage is finally formed.

To further illustrate the effect of the imperfection in hydrogenation on the kinetics of nanocage formation, Figure S4 (c) compares the energy evolution of the simulated structure under hydrogenation perfection rates of 100% (complete hydrogenation, as in Figure 2 (c)), 89.2%, 78.3% and 69.9%, respectively. Figure S4 (a) and (b) show the defective hydrogenation pattern with the perfection rate of 89.2% and 78.3%, respectively, and also the final shape of the resulting nanocage structure. Similar significant drops of energy as the patterned graphene folds up and the nanocage forms occur in all four cases. The time needed to form a graphene nanocage as well as the equilibrium energy level increases slightly as the hydrogenation perfection rate decreases. Nonetheless, all curves in Figure S4 (c) suggest that the HAGO-driven process of patterned graphene with defective hydrogenation is energetically favorable. To further demonstrate the robustness of HAGO-driven process is insensitive to the randomness of the

defective hydrogenation, Figure S5 shows another set of three randomly generated defective hydrogenation patterns with perfection rate of 89.2%, 78.3%, and 69.9%, respectively, all of which leads to successful formation of a graphene nanocage in a similar fashion as shown in Figures S3 and S4.

The above studies clearly demonstrate that HAGO is a rather robust self-assembly process with a strong tolerance to possible imperfect hydrogenation in practices.

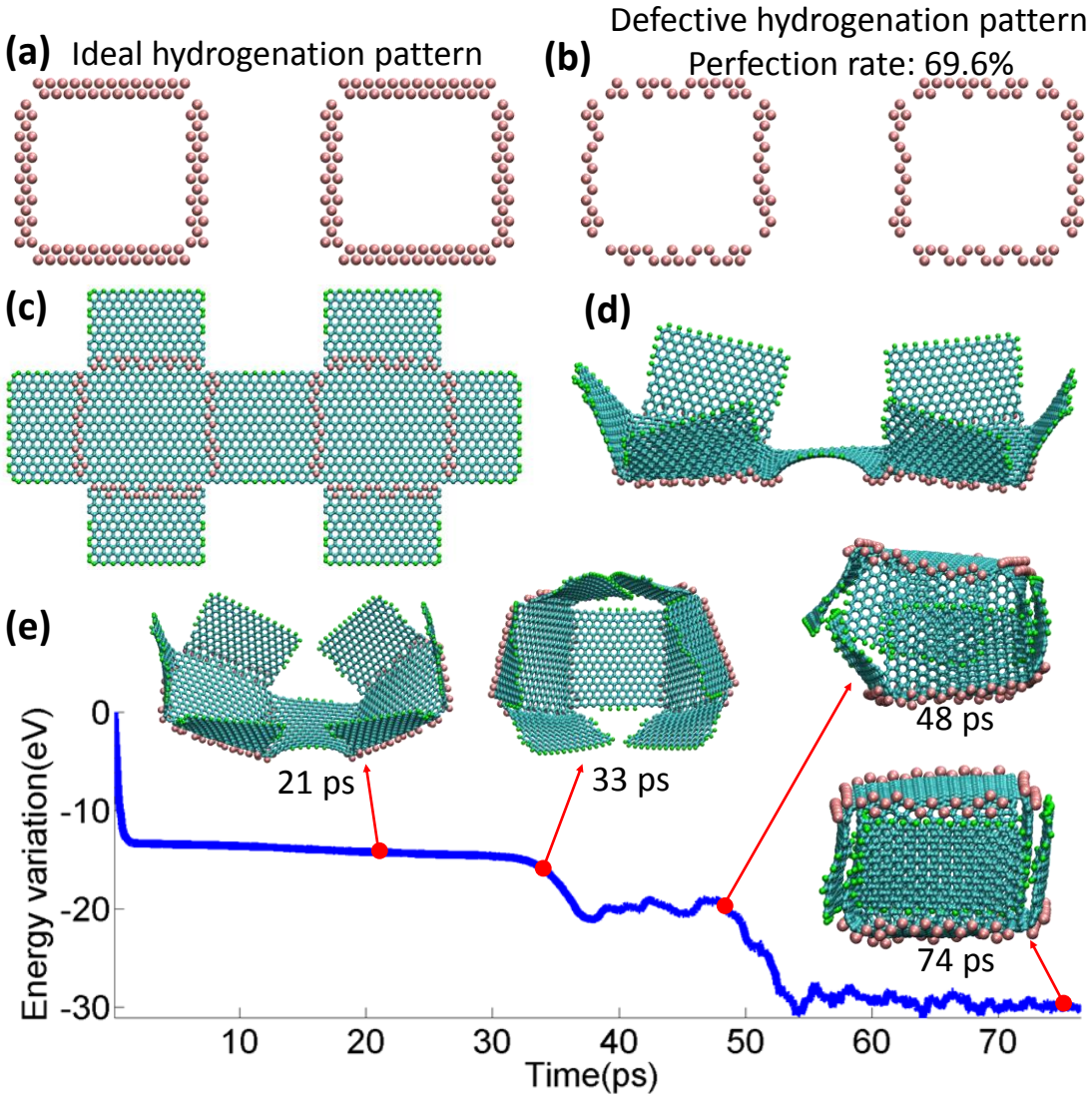

Figure S3. *(a) Complete single-sided hydrogenation pattern, with 184 hydrogen atoms, as in Figure 2. For visual clarity, only hydrogen atoms are shown. (b) A randomly generated defective hydrogenation pattern, which contains 128 hydrogen atoms (i.e., the perfection rate is 69.6%). (c)*

Double-cross shaped graphene flake with the defective hydrogenation pattern of (b). (d) Energy-minimized structure in (c) by conjugate gradient and steepest descent algorithm. (e) Further energy minimization towards the formation of a graphene nanocage.

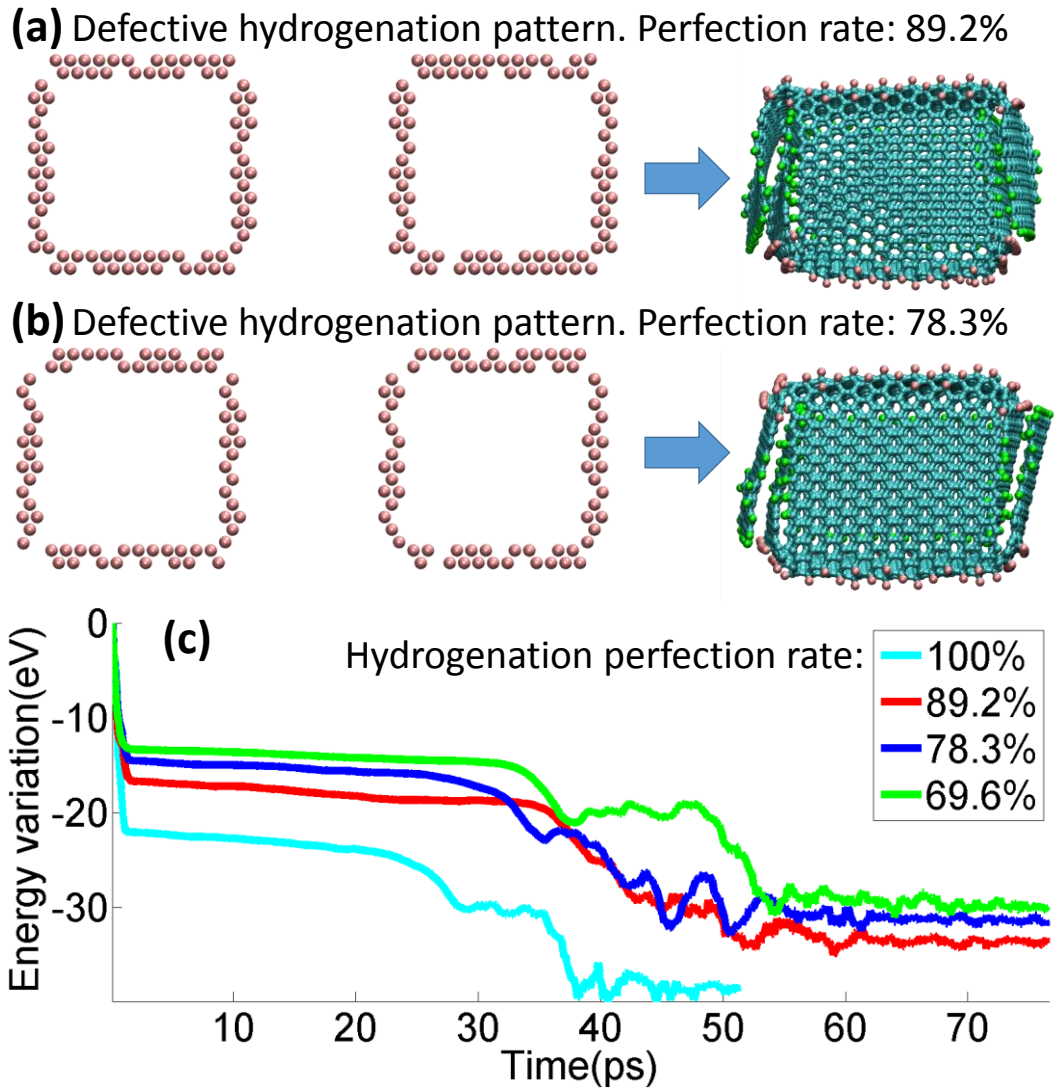

Figure S4. *(a) Randomly generated defective hydrogenation pattern with 164 hydrogen atoms (perfection rate 89.2%) and its resulting graphene nanocage. (b) Randomly generated defective hydrogenation pattern with 144 hydrogen atoms (perfection rate 78.3%) and its resulting graphene nanocage. (c) Comparison of the energy evolution for different hydrogenation perfection rates towards the formation of nanocage. The curve for 100% perfection rate is replotted from Figure 2 (c) for comparison.*

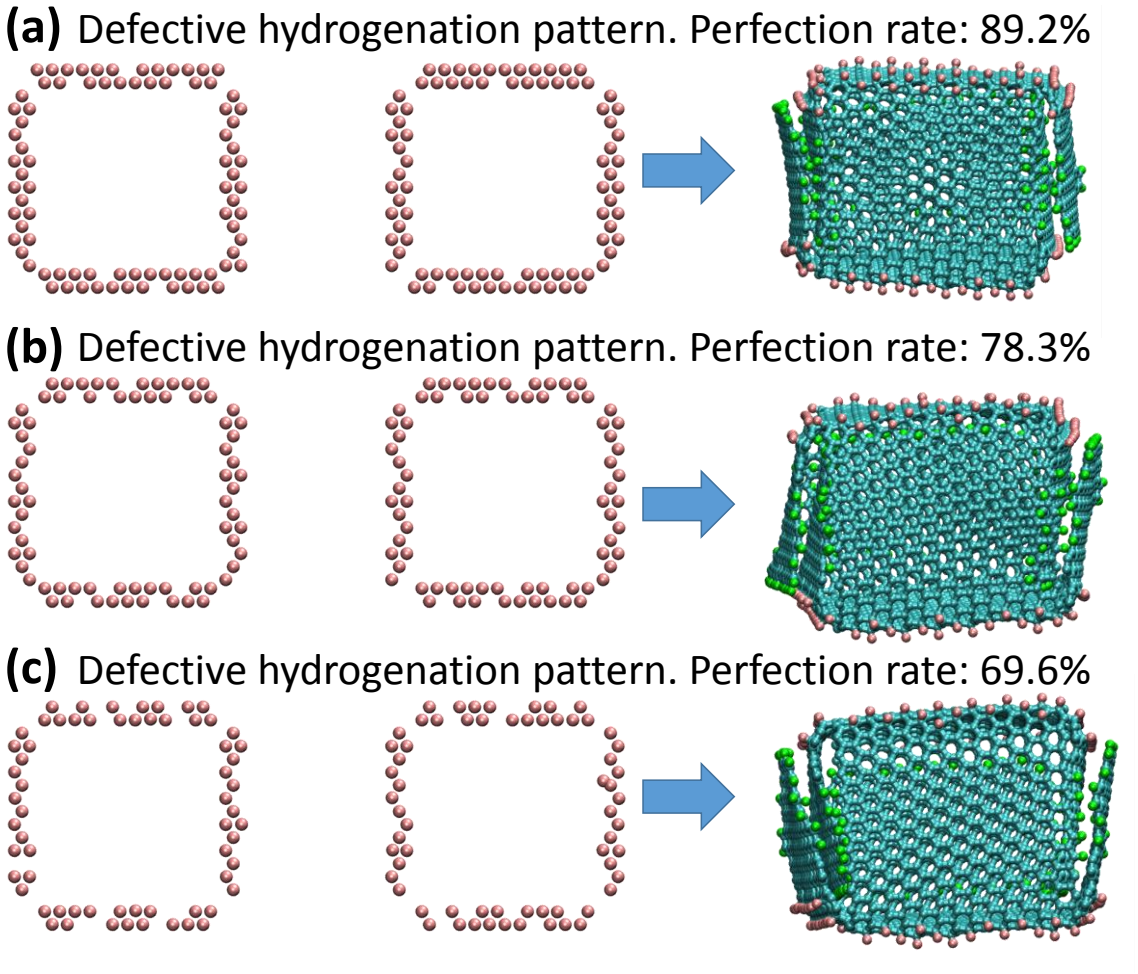

Figure S5. *Another set of randomly generated defective hydrogenation patterns and their resulting graphene nanocages. Hydrogenation perfection rate: (a) 89.2%. (b) 78.3%. (c) 69.6%.*

V. Effect of hydrogenation and folding induced global polarization on the morphology of graphene nanocage under an external electric field

Beside the local point dipoles induced by an external electric field, intrinsic global polarization could also occur in a HAGO-enabled nanostructure. Such an intrinsic polarization results from the non-uniform distribution of charges in the resulting nanostructures due to hydrogenation and folding. Figure S6 (a) shows the charge distribution in the resulting graphene nanocage. The initial charge for every atom in the graphene nanocage structure is set to zero. The equilibrium

charge distribution is calculated by the ReaxFF potential implemented in LAMMPS package. Due to the difference of electronegativity between hydrogen and carbon atoms, the hydrogen atoms that reside on the edges of the nanocage have the highest positive charge; The carbon atoms that are bonded to those hydrogen atoms have the highest negative charge while other carbon atoms have charges with extremely low magnitude. Subject to an external electric field, the positively charged hydrogen atoms and the negatively charged carbon atoms that are bonded to these hydrogen atoms would experience local electrostatic forces in opposite directions. As a result, the folded edges in the nanocage would subject to localized electrostatic moments. Figure S6 (b) further clarifies the distribution of the positive and negative charges in the nanocage, which adopts an alternating pattern. For example, most part of the top surface is negatively charged, while the edges are positively charged. Similarly, the middle portion of the side surface is negatively charged, while the edges and some portion near the edges are positively charged. Such alternating polarization patterns give rise to the formation of large molecular dipoles within the nanocage. An external electric field can interact with such dipoles and thus change the morphology of the graphene nanocage. To demonstrate such an effect of external electric field on the morphology change of the graphene nanocage, we explicitly prescribe a constant electric field in the MD simulation, which is carried out in NVT ensemble at a temperature of 300K. The electric field is assigned along a fixed direction and the effect of electric field intensity is studied.

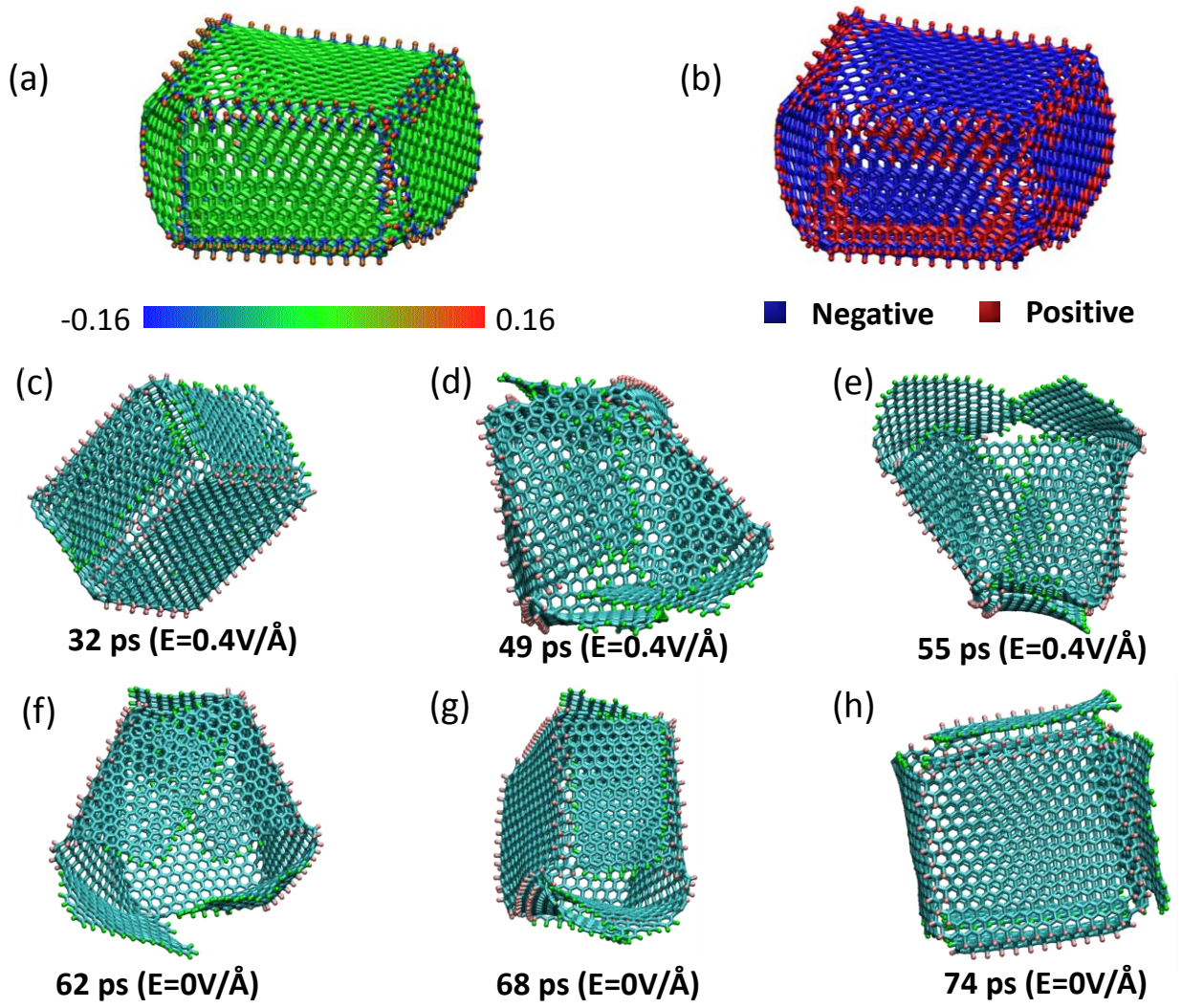

Figure S6. *(a) Hydrogenation and folding induced non-uniform charge distribution in the graphene nanocage. (b) Mapping of positive and negative charges in the graphene nanocage. (c)-(e) The opening process of the graphene nanocage under the electrostatic force induced by an external electric field. (f)-(g) Upon removing the external electric field, the partially open graphene nanocage closes up spontaneously.*

Subject to a weak electric field (*e.g.*, with an intensity of 0.1V/Å), no appreciable morphology change of the nanocage is observed as the resulting electrostatic force or moment is not strong enough to overcome the stabilizing interactions such as inter-wall vdW forces. However, subject to an electric field of intensity of 0.4V/Å, the graphene nanocage becomes unstable and fails to

maintain its hexahedral shape. Figure S6 (c) to (e) show the sequential snapshots of the resultant opening process of the graphene nanocage under such an electric field. When the electric field is turned off after the nanocage opens up, the partially unfolded structure can gradually recover its hexahedral configuration, as shown in Figure S6 (f) to (h). The above analysis reveals that the hydrogenation and folding induced intrinsic polarization of the graphene nanocage indeed facilitates the programmable opening of the nanocage via an external electric field.

Section VI: Hydrogen storage process in a graphene nanocage immersed in a hydrogen reservoir

We investigate the hydrogen storage process using a graphene nanocage. Figure S7 (a) shows the simulation model, an initially empty cubic graphene nanocage (about 3 nm by 3 nm by 3 nm) formed by HAGO process is placed in a hydrogen reservoir with a cubic cavity of proper size to fit the nanocage. A cubic simulation box (8.6 nm by 8.6 nm by 8.6 nm) is used with periodical boundary condition prescribed in all three principal directions. Effectively, such a simulation models the senario of a large number of empty graphene nanocages immersed in a vast hydrogen reservoir in a periodical fashion. The simulation is done in 70K in NVT ensemble and by Nose-Hoover thermostat. Figure S7 (b) shows a typical cross-section view of the hydrogen reservoir when the nanocage remains closed in a dynamics simulation (for visual clarity the nanocage is not shown). Figure S7 (b) shows a cross-section view of the hydrogen reservoir when the nanocage remains closed in simulation. When an electric field is applied ($i.e., \lambda_{CC} = 0.05$ in Figure S7(c)), the slight opening of the nanocage against the outer pressure from the hydrogen reservoir creates gaps and pores along the edges and corners of the nanocage, through which the hydrogen can diffuse into the inner volume of the nanocage. Figure S7 (d) shows several

snapshots of the cross-section views of the hydrogen reservoir, revealing the gradual adsorption process of hydrogen into the inner volume of the nanocage. The adsorption process lasts for 400 ps, during which the electric field is first on for 50 ps and then off for 50 ps, and such a pattern is repeated during the 400 ps.

Figure S7 (e) further plots the number of hydrogen atoms adsorbed into the nanocage and the corresponding weighted percentage of hydrogen storage at four stages shown in Figure S7 (d). It is shown that, a weighted percentage of hydrogen storage of 2.51% can be achieved using a graphene nanocage with a dimension about 3 nm by 3 nm by 3 nm. This weighted percentage is smaller than that shown in Figure 7 (a) due to the relatively smaller nanocage dimension used here. Figure S7 (f) plots the evolution of the effective volume density of hydrogen adsorbed inside the graphene nanocage, which shows an increasing trend of the hydrogen volume density inside the nanocage. At the equilibrium, the hydrogen atoms adsorbed inside the nanocage reaches a volume density comparable to the ambient hydrogen volume density (defined as the total number of hydrogen atoms in the simulation box divided by the volume of the simulation box). This result suggests that it is possible to tune the hydrogen storage density in graphene nanocage by varying the pressure of the hydrogen reservoir (*e.g.*, a higher storage density achieved by increasing the reservoir pressure), a desirable feature for hydrogen storage.

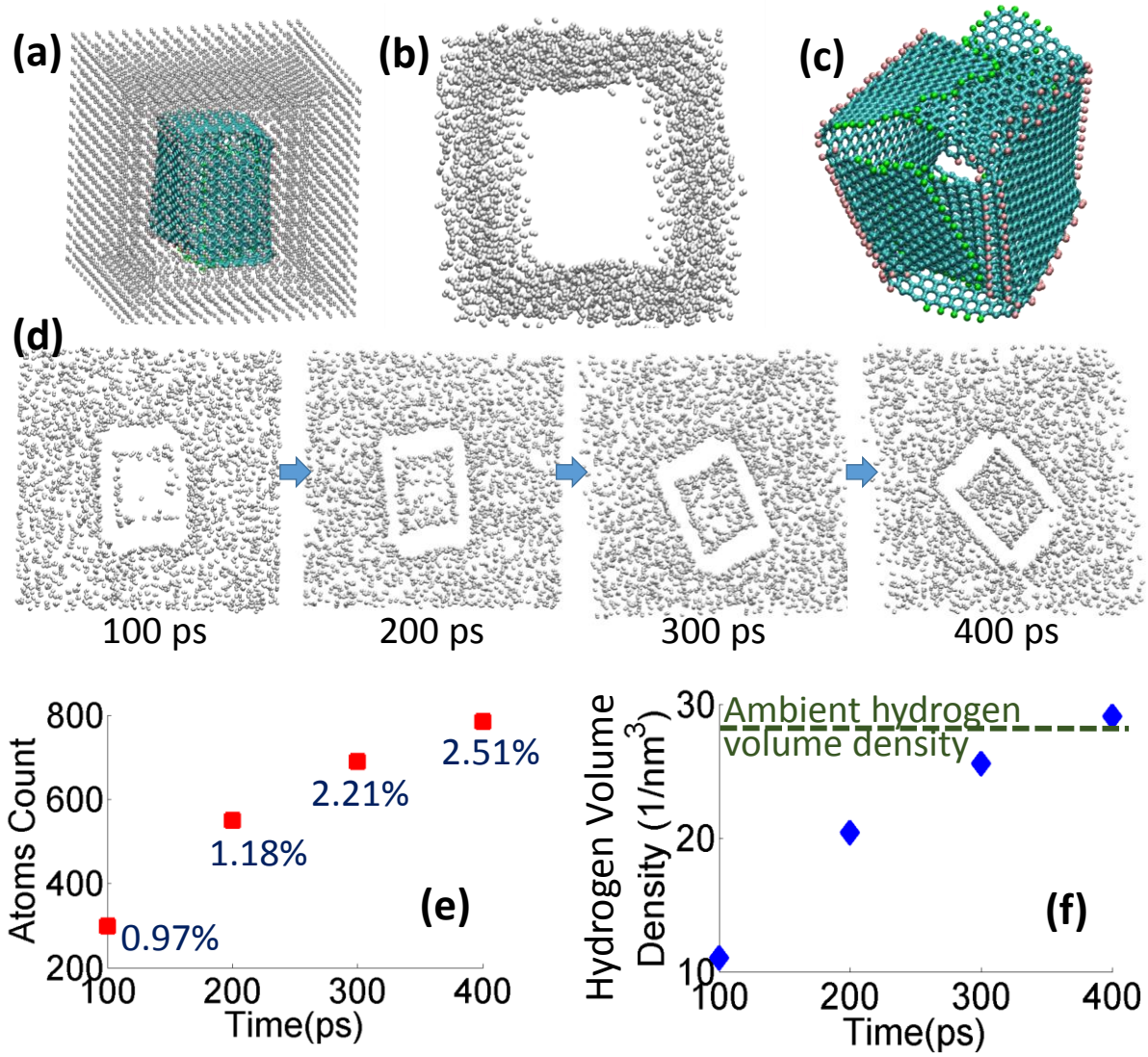

Figure S7. *(a) Simulation model of an empty graphene nanocage immersed in a hydrogen reservoir. (b) A cross-section view of the hydrogen reservoir when the graphene nanocage is closed in a dynamics simulation (for visual clarity, the nanocage is not shown). (c) The slight opening of graphene nanocage gives rise to gaps and pores along the edges and corners. For visual clarity, the ambient hydrogen atoms are not shown. (d) Sequential snapshots of the cross-section view of the hydrogen reservoir showing the adsorption of hydrogen into the inner volume of the nanocage. For visual clarity, the nanocage is not shown. (e) The evolution of the number of hydrogen atoms adsorbed into the nanocage and the corresponding weighted percentage of hydrogen storage. (f) The evolution of the effective volume density of hydrogen adsorbed inside the graphene nanocage. The dashed shows the level of ambient volume density of hydrogen atoms.*

VII. Temperature-modulated release of hydrogen atoms from graphene nanocage

To demonstrate a feasible and safe approach to releasing the hydrogen atoms stored in the graphene nanocage (*e.g.*, Figure 7 (a)), we further investigate the effect of temperature on hydrogen release. When the temperature is elevated, the kinetic energy of the hydrogen atoms increases. As a result, the pressure exerted by the hydrogen to the graphene nanocage increases. Since the graphene nanocage is not covalently bonded but rather sealed via vdW interaction, the increase in the kinetic energy of the hydrogen atoms could eventually outweigh the vdW adhesion energy that holds the graphene nanocage if the temperature is sufficiently high. As a result, the graphene nanocage could partially open up so that hydrogen atoms can escape from the nanocage. To demonstrate the above effect, we use the hydrogen-filled graphene nanocage structure in Figure 7 (a) as the starting configuration and perform molecular dynamics simulations in NVT ensemble to increase the temperature to 300 K by Nose-Hoover thermostat. As shown in Figure S8, at a higher temperature, the four edges of the graphene nanocage that are not covalently sealed start to open up under the increased internal pressure from the hydrogen atoms. As a result, pressurized hydrogen atoms spray out from the open edges. At 193 ps, majority of the hydrogen atoms initially stored inside the graphene nanocage are successfully released and fill up the entire simulation box. These results suggest that elevating temperature can be an effective and feasible mechanism to release the hydrogen atoms stored inside the graphene nanocage.

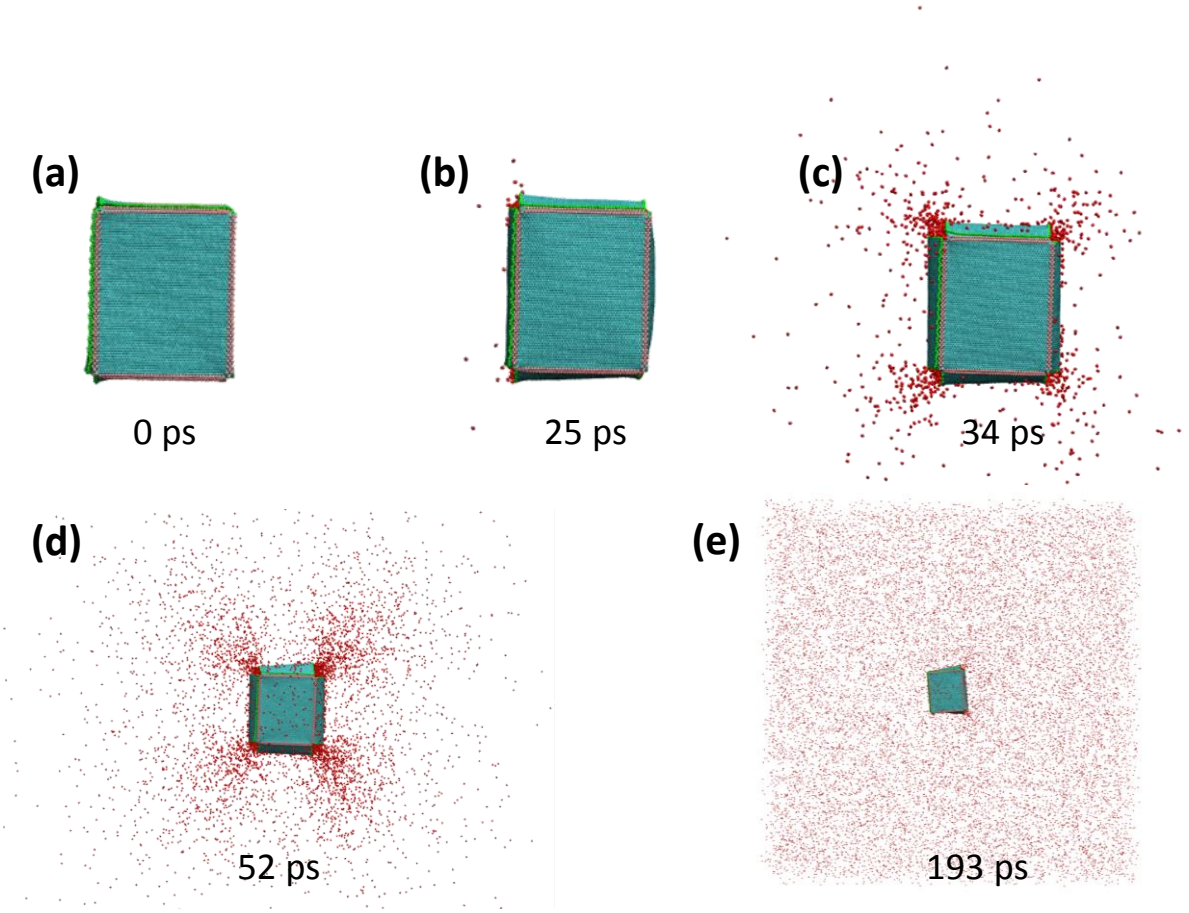

Figure S8. *Release of hydrogen stored inside a graphene nanocage at an elevated temperature (300K). Starting configuration is the same structure as in Figure 7 (a). Increasing pressure of stored hydrogen at elevated temperature causes the partial opening of the four edges of the graphene nanocage that are not covalently sealed, which allows the hydrogen atoms to spray out. After 193 ps, majority of stored hydrogen atoms are released. The simulation is in NVT ensemble and by Nose-Hoover thermostat. Hydrogen molecules are colored in red.*

References:

S1. Shi, X.; Cheng, Y.; Pugno, N.; Gao, H. Tunable Water Channels with Carbon Nanoscrolls. *Small* **2010**, *6*, 739-744.

VIII. Supplementary Movies

Movie M1. Initial energy minimization of the patterned graphene (corresponding to Figure 2 (b))

Movie M2. HAGO-enabled formation of a hexahedral graphene nanocage (corresponding to Figure 2 (c))

Movie M3. Controlled opening and closing of HAGO-enabled graphene nanocage via an external electric field (corresponding to Figure 4)

Movie M4. Uptake of a C60 molecule by graphene nanocage via controlled opening and closing (corresponding to Figure 5 (a-d))

Movie M5. Release of the trapped C60 molecule via controlled opening and closing of the graphene nanocage (corresponding to Figure 5 (e-h))

Movie M6. HAGO-enabled formation of a large graphene nanocage (corresponding to Figure 6 (b-f))

Movie M7. High density hydrogen storage in a HAGO-enabled graphene nanocage (corresponding to Figure 7 (a))